Journal of Neuroinflammation

RESEARCH

Open Access

Inhibition of histone deacetylase 6 alleviates neuropathic pain via direct regulating post-translation of spinal STAT3 and decreasing downstream C-C Motif Chemokine Ligand 7 synthesis

Zhexi Chi[1†], Bo Lu[1†], Rongjun Liu[1], Chen Pan[2], Bo Meng[3], Xiuzhong Xing[3], Hui Yuan[3], Xuewei Wu[2], Yushan Chen[2], Yuxuan Ren[2], Wenwei Wu[2], Mengmeng Miao[2], Junping Chen[1*] and Xiaowei Chen[2*]

Abstract

Neuropathic pain, a debilitating nerve injury-induced condition, remains a significant clinical challenge. This study evaluates the effect of histone deacetylase 6 (HDAC6) inhibition in a spared nerve injury (SNI) mouse model. Systemic administration of the selective HDAC6 inhibitor ACY-1215 (20 mg/kg/day, 14 days), alleviated SNI-induced pain in mice of both sexes. ACY-1215 increased acetylated signal transducer and activator of transcription 3 (Ac-STAT3) and reduced phosphorylated STAT3 (p-STAT3) in the lumbar spinal cord of SNI mice. HDAC6 and p-STAT3 were expressed in spinal dorsal horn neurons, and SNI-enhanced HDAC6/STAT3 interaction was reversed by ACY-1215. Neuronal STAT3 overexpression induced pain hypersensitivity and elevated p-STAT3, tumor necrosis factor-alpha (TNF-α) and interleukin-1 beta (IL-1β), effects suppressed by ACY-1215. Cytokine profiling identified CC-chemokine ligand 7 (CCL7) as a key downstream effector of the HDAC6/STAT3 axis, with ACY-1215 attenuating SNI-induced CCL7 upregulation. HDAC6 knockdown in neurons reduced p-STAT3, while HDAC6 or STAT3 knockdown diminished CCL7 production. These findings demonstrate that ACY-1215 mitigates neuropathic pain by modulating STAT3 acetylation/phosphorylation and suppressing HDAC6/STAT3-driven CCL7 and cytokine release. This study underscores the role of the HDAC6/STAT3/CCL7 signaling axis in neuropathic pain and highlights the therapeutic potential of HDAC6 inhibitors for pain management.

Keywords Neuropathic pain, HDAC6, ACY-1215, STAT3, CCL7

†Zhexi Chi and Bo Lu contributed equally to this work.

*Correspondence:
Junping Chen
13858222873@163.com
Xiaowei Chen
chenxiaowei@nbu.edu.cn

[1]Department of Anesthesiology, Ningbo No. 2 Hospital, Ningbo, Zhejiang 315010, China
[2]Health Science Center, Ningbo University, Ningbo, Zhejiang 315211, China
[3]Department of Pain, Ningbo No. 2 Hospital, Ningbo, Zhejiang 315010, China

Introduction

Neuropathic pain results from injury or dysfunction of the nervous system, characterized by pathological changes in sensory processing. It is a significant global health issue, affecting an estimated 7–10% of the population worldwide [1, 2]. A recent large-scale epidemiological study involving over 148,000 participants from the UK Biobank reported a neuropathic pain prevalence of 9.2%, with chronic pain affecting 51.1% of the cohort [3]. Clinically, neuropathic pain manifests as spontaneous pain, hyperalgesia, allodynia, and paresthesia, significantly impairing patients' quality of life [4]. Current pharmacological management of neuropathic pain includes antiepileptic drugs (e.g., gabapentin, pregabalin), antidepressants (e.g., amitriptyline, venlafaxine), and other agents such as opioids and lidocaine patches [5]. However, these treatments often provide limited efficacy and are associated with side effects, highlighting the need for more effective and safer therapeutic strategies [6]. Consequently, identifying novel molecular targets and developing innovative interventions for neuropathic pain remain critical priorities in pain research.

Histone deacetylase (HDAC) enzymes play a key role in regulating gene expression, primarily through the deacetylation of histones and modulation of chromatin structure, which in turn influences transcriptional activity [7]. Beyond histones, HDACs also target non-histone proteins, including tubulin, p53, and signal transducer and activator of transcription 3 (STAT3) [8–10]. Dysregulation of HDAC activity has been implicated in various diseases, including cancer, neurodegenerative disorders, and inflammatory conditions. Notably, several HDAC inhibitors have already been approved for clinical use in cancer therapy, underscoring their therapeutic potential [11].

Among HDACs, histone deacetylase 6 (HDAC6) is a class II HDAC, specifically deacetylates non-histone substrates. HDAC6 is involved in various physiological and pathological processes [12, 13]. Emerging evidence highlights the role of HDAC6 in neurological diseases, including pain [14–17]. HDAC6 inhibitor ACY-1215 (Ricolinostat) mitigates mechanical allodynia induced by peripheral nerve injury [14] or inflammation [15]. Additionally, HDAC6 inhibitors, including ACY-1215, exhibit brain permeability, suggesting their therapeutic potential in treating neurological disorders [18]. However, the pharmacological actions and mechanisms of HDAC6 inhibitors in neuropathic pain remain incompletely understood. In particular, the potential modulation of non-histone proteins and their downstream signaling pathways in the context of neuropathic pain requires further investigation.

Signal transducer and activator of transcription 3 (STAT3), a member of the STAT family of transcription factors, is activated through phosphorylation and subsequently translocates to the nucleus, where it regulates the expression of multiple genes in response to stimuli [19, 20]. In recent years, STAT3 has emerged as a critical player in the development and maintenance of neuropathic pain [19, 21, 22]. In the spinal cord, activation of glial STAT3 promotes neuroinflammation and neuronal hyperexcitability, both of which contribute to chronic pain [22]. STAT3 activation facilitates the release of inflammatory factors, including tumor necrosis factor-alpha (TNF-α), interleukin-1 beta (IL-1β), and interleukin-6 (IL-6), which exacerbate pain signaling [23–25]. While pharmacological inhibition of STAT3 has been shown to alleviate neuropathic pain, the precise mechanisms remain incompletely understood, and the use of STAT3 inhibitors is limited by potential cytotoxic effects [21, 26]. As an alternative, targeting post-translational modifications of STAT3 may offer a safer therapeutic approach. Although previous studies have examined the effects of an HDAC inhibitor on STAT3 mRNA transcription [27], the direct interaction between HDAC6 and STAT3 in the nervous system has not been explored. Furthermore, it remains unclear whether the anti-nociceptive effects of HDAC6 inhibitors involve the post-translational regulation of STAT3.

Recent studies have highlighted a critical link between STAT3 activation and the production of cytokines and chemokines [28]. In neuropathic pain, emerging evidence suggests that chemokines are upregulated in both the peripheral and central nervous systems following nerve injury, contributing to neuroinflammation and the sensitization of nociceptive pathways [28–30]. However, the specific downstream cytokines or chemokines regulated by STAT3 in response to HDAC6 inhibition have yet to be identified. Elucidating these downstream effectors could provide valuable insights into the HDAC6/STAT3 signaling axis and its role in neuropathic pain.

In the present study, we employed a spared nerve injury (SNI) model to investigate the anti-nociceptive effects of the selective HDAC6 inhibitor ACY-1215. We examined the interaction between HDAC6 and STAT3 and identified downstream cytokines and chemokines within the HDAC6/STAT3 signaling pathway. Our findings shed light on the mechanisms by which HDAC6 regulates post-translational modifications of STAT3 in neuropathic pain and underscore the therapeutic potential of HDAC6 inhibitors for pain management.

Materials and methods

Animals

Male and female CD-1 mice (6–8 weeks, 20–25 g) were purchased from Beijing Vital River Laboratory Animal Technology Co (Pinghu, Zhejiang, China). The mice were housed in a temperature-controlled animal facility with a 12 h light–dark cycle and ad libitum access to food and

water. Criteria for exclusion included weight loss, disability or distress. All procedures were approved by the Animal Care and Use Committee of Ningbo University in accordance with the National Institutes of Health Guidelines for the Care and Use of Laboratory Animals (NIH Publications No. 80 – 23). Female mice were only used in the behavioral tests.

Chemicals and antibodies

ACY-1215 was purchased from Medchemexpress (Hong KONG, China) and dissolved in 10% dimethyl sulfoxide (DMSO), obtained from Sigma-Aldrich (St. Louis, MO, USA). Lipofectamine 2000 Transfection Reagent and Opti-MEM I were purchased from Thermo Fisher Scientific Life Sciences (Waltham, MA, USA). Dulbecco's Modified Eagle Medium, Fetal bovine serum (FBS) and penicillin/streptomycin were obtained from HyClone (Logan, UT, USA). Recombinant Mouse IL-6 was purchased from ABclonal (RP01321, Ningbo, China). Antibodies against HDAC6 (#7558), STAT3 (#9139), Acetyl-STAT3 (Lys685, #2523), Phospho-STAT3 (Tyr705, D3A7, #9145), Acetyl-α-Tubulin (Lys40, D20G3, #5335), α-Tubulin (#2144), IL-1β (3A6, #12242), TNF-α (D2D4, #11948), and GFAP (Cat#3670) were purchased from Cell Signaling Technology (Danvers, MA, USA). Antibodies against Anti-CGRP (#ab81887), IBa-1(Cat#ab5076), and Lamin B1 (#ab65986), and the secondary antibody AlexaFluor 488, donkey anti-goat (Cat#ab150129) were purchased from Abcam (Cambridge, MA, USA). Neuronal marker NeuN (Cat#N21483) and IB4 (Cat#I32450), and antibody against CCL7 (Cat#38675A01) were purchased from Thermo Fisher Scientific (Waltham, MA, USA). The secondary antibody Goat anti-rabbit IgG antibody (Cat#A0208) and goat anti-mouse IgG antibody (Cat#A0216) were purchased from Beyotime (Shanghai, China). Other secondary antibodies including AlexaFluor 488, donkey anti-mouse (Cat#715-545-150), AlexaFluor 594, donkey anti-rabbit (Cat#711-585-152), and AlexaFluor 488, donkey anti-rabbit (Cat#711-545-152) were purchased from Jackson ImmunoResearch Inc. (West Grove, PA, USA).

Establishment of spared nerve injury (SNI) model

The SNI surgery was performed as previously described [31, 32]. Male and female mice were anesthetized with sodium pentobarbital (50 mg/kg, Aladdin, Shanghai, China). The right sciatic nerve was exposed at the mid-thigh region proximal to the sciatic trifurcation. Subsequently, the common peroneal and tibial nerves were ligated and excised, while the sural nerve remained intact. Sham surgery was performed without damaging the nerve, involving only exposure without lesioning.

Von frey test

The Von Frey tests were performed to evaluate mechanical pain thresholds as previously described [33–36]. Briefly, mice were placed in individual transparent Perspex cubicles with a wire mesh base and allowed at least 20 min to acclimate. The filaments were applied to the plantar surface of the right hind paw in a series of ascending forces. Mechanical thresholds were determined using the up-and-down method with Von Frey filaments (Stoelting, USA).

Cell cultures and treatments

Mouse hippocampal cells (HT22) were obtained from the Chinese Academy of Sciences (Shanghai, China) and cultured in Dulbecco's Modified Eagle Medium (DMEM) supplemented with 10% FBS and penicillin/streptomycin. The cell cultures were maintained at 37 °C in a humidified atmosphere containing 5% CO_2 and 95% air. Subculturing was routinely performed every 2 or 3 days. For sample preparations, an equal number of cells were seeded into culture dishes at a density of 5×10^4 cells/cm^2 overnight. In the case of IL-6 treatment, cells were incubated with a final concentration of 100 ng/ml of IL-6 for 12 h.

Construction of STAT3 overexpression

The STAT3 overexpression plasmid (Cat#PT7722) was constructed, and recombinant adeno-associated virus 2/9 vector carrying STAT3 overexpression plasmid with human synapsin (hSyn) neuronal promoter (AAV-hsyn-STAT3-EGFP) or the vacant controls (AAV-hsyn-EGFP) were packaged by BrainVTA (Wuhan, China).

Mice were anesthetized with Avertin (20 mg/ml, 0.2 ml per 10-gram weight). The skin overlying the spinal column was then shaved and cleaned to reduce the risk of infection. A small incision was made in the skin and a 30-gauge needle was inserted into the subarachnoid space between the L4-L6 vertebrae and around the spinal cord. The virus emulsion (10^{12} vg/mL, 5 μl in PBS) containing the AAV-hsyn-STAT3-EGFP or AAV-hsyn-EGFP was then intrathecally injected slowly and carefully into the space. After the injection, the incision was closed and the mice were allowed to recover. The mice were closely observed for any discomfort or complications after surgery.

Plasmid transfection and gene knockdown

HT22 cells were transfected with expression plasmids of HDAC6 or STAT3 small interfering RNA (siRNA) or control siNRA using Lipofectamine 2000 for 2 days following manufacturer's instructions. HDAC siRNA(5′-AGA CCU AAU CGU GGG ACU GCT T-3′), STAT3 siRNA (5′-GGG ACC UGG UGU GGG AAU UAU TT-3′) or a scramble negative control (5′-UUC UCC GAA CGU GUC ACG UTT-3′) from GenePharma

(Shanghai, China) were mixed with Lipofectamine 2000 in Opti-MEM I, and the mixtures were added to cells for 48 h.

Western blotting and co-immunoprecipitation (Co-IP)

For experiments involving spinal cord tissue, mice were humanely killed by CO_2 inhalation. The L4-6 spinal dorsal horn tissues were dissected and homogenized in an ice-cold RIPA lysis buffer (Cat# P0013B; Beyotime, Shanghai, China) supplemented with protease and phosphatase inhibitors (Cat#A32959, Thermo Fisher). The homogenates were centrifuged at 13,200 rpm for 30 min at 4 °C. For experiments using H22 cells, cells were lysed in the RIPA lysis buffer containing the same protease and phosphatase inhibitors, followed by centrifugation under identical conditions to obtain the supernatant. Protein concentration was determined using the BCA Protein Assay Kit (Beyotime, Beijing, China). The samples were separated on 8–10% SDS-PAGE gels and transferred to PVDF membranes (Millipore, Temecula, CA, United States) [37]. Membranes were blocked with 5% skim milk in TBST buffer (20 mM Tris, 150 mM NaCl, 0.1% Tween 20; Sigma-Aldrich, USA) and subsequently incubated overnight at 4 °C with primary antibodies diluted in TBST. The following primary antibodies were used: HDAC6 (1:1000), Ac-STAT3 (1:1000), p-STAT3 (1:1000), STAT3 (1:1000), Ac-α-Tubulin (1:1000), Tubulin (1:1000), Lamin B1 (1:1000), TNF-α (1:1000), IL-1β (1:1000), and CCL7 (1:1000). After washing with TBST, membranes were incubated for 1 h at room temperature with species-appropriate secondary antibodies: goat anti-rabbit IgG (1:1000) or goat anti-mouse IgG (1:1000). Between detections, membranes were stripped using Western Blot Fast Stripping Buffer (Cat#PS107, Epizyme Biomedical Technology Co, Shanghai, China). Target bands were visualized using an Odyssey Infrared Imaging System (LI-COR Biotechnology, NE, USA), and band intensities were quantified using ImageJ analysis software (NIH, USA).

Co-IP of STAT3 was performed using an anti-STAT3 mouse monoclonal antibody, with normal mouse IgG serving as a negative control. Immune complexes were captured with 25 µl of Protein A/G PLUS-Agarose IP reagent (Santa Cruz Biotechnology, United States) for 2 h and washed 5 times with the lysis buffer [38]. The starting tissue lysates and IP products were separated on 8–10% SDS-PAGE gels and transferred to PVDF membranes (Millipore, Temecula, CA, United States). Target proteins were probed with the following primary antibodies HADC6 (1:1000), Ac-STAT3 (1:1000), STAT3 (1:1000). After washing, membranes were incubated with horseradish peroxidase-conjugated secondary antibodies Goat anti-rabbit IgG antibody (1:1000) or goat anti-mouse IgG antibody (1:1000). Protein bands were visualized using an Odyssey Infrared Imaging System (LI-COR Biotechnology, NE, USA), and band intensities were quantified using ImageJ analysis software (NIH, USA).

Cytosol and nuclear fractionation

On the 14th day post-SNI or sham surgery, mice were humanely killed by CO_2 inhalation. The L4-6 spinal dorsal horn tissues were collected and homogenized in an ice-cold lysis buffer (Cat#P0013B; Beyotime, Shanghai, China) containing protease and phosphatase inhibitors (Cat#A32959, Thermo Fisher). The homogenates were centrifuged at 13,200 rpm for 30 min at 4 °C to obtain the supernatant. Cytoplasmic and nuclear protein fractionation were isolated using a Nuclear Extraction Kit (#2900, Merck Millipore, United States) according to the manufacturer's protocol. The purity of the cytosolic and nuclear fractions was examined by Western blot analysis using primary antibodies targeting α-Tubulin (1:1000; cytosolic marker) and Lamin B1 (1:1000; nuclear marker) [7], followed by species-appropriate secondary antibodies: goat anti-rabbit IgG antibody (1:1000) or goat anti-mouse IgG antibody (1:1000). Protein bands were detected using an Odyssey Infrared Imaging System (LI-COR Biotechnology, NE, USA), and band intensities were quantified using ImageJ analysis software (NIH, USA).

Enzyme-linked immunosorbent assay (ELISA)

The ELISA was performed as previously described [36]. On the 14th day post-SNI or sham surgery, mice were humanely killed by CO_2 inhalation and L4-6 spinal cords were harvested. Tissue were rinsed with cold PBS and homogenized for ELISA assays of (#E-MSEL-M0002, Elabscience, China), IL-1β (#E-MSEL-M0003, Elabscience, China), and CCL7 (#ab250071, Abcam, Cambridge, MA, USA). Reagents and working standards were prepared according to the manufacturer's instructions, and the assay was performed following the provided protocol. Absorbance was measured at 450 nm using a microplate spectrophotometer (Thermo Inc, USA).

Multiplex cytokine and chemokine analysis

On day 14 post-SNI or sham surgery, mice from the Sham, SNI, and SNI + ACY-1215 groups were euthanized humanely via CO_2 inhalation. The L4–L6 spinal cord tissues were collected, homogenized in ice-cold lysis buffer (Cat#P0013B; Beyotime, Shanghai, China) containing protease and phosphatase inhibitors (Cat#A32959, Thermo Fisher), and centrifuged at 13,200 rpm for 30 min at 4 °C. Protein concentrations were determined using a BCA Protein Assay Kit (Beyotime, Beijing, China).

Multiplex cytokine and chemokine analysis was performed using the Bio-Plex Pro Mouse Chemokine Panel 31-plex (BIO-RAD Lab, Inc, Hercules, CA, USA). The assay was conducted according to the manufacturer's

instruction, and individual samples from each mouse in each group were analyzed.

Immunofluorescence and image analysis

Mice were anesthetized with Avertin (20 mg/ml, 0.2 ml per 10-gram weight) and intracardially perfused with saline followed by 4% paraformaldehyde (Solarbio, Beijing, China, Cat. No. P1110) in 0.1 M phosphate buffer. The L4-6 spinal tissue was dissected, fixed in 4% paraformaldehyde overnight at 4 °C, and sequentially transferred to 15% and then 30% sucrose in 0.1 M phosphate buffer solution at 4 °C. Tissues were sectioned at 20 μm using a cryostat (CM1950, Leica, Germany). Sections were blocked with 10% normal donkey serum in 0.01 M phosphate-buffered saline containing 0.3% Triton X-100 (Cat#P0096; Beyotime, Shanghai, China) for 1 h at room temperature. Spinal cord sections were then incubated overnight at 4 °C with the following primary antibodies or marker: HACD6 (1:100), p-STAT3 (1:100), GFAP (1:200), Iba-1 (1:200), CGRP (1:200), NeuN (1:200), IB4 (1:500). After washing by PBST (PBS with 0.1% Tween20, Solarbio, Beijing, China), sections were incubated for 2 h at room temperature with the species-appropriate secondary antibodies: AlexaFluor 488, donkey anti-mouse (1:400), AlexaFluor 594, donkey anti-rabbit (1:400), AlexaFluor 488, donkey anti-rabbit (1:400), AlexaFluor 488, donkey anti-goat (1:200). Sections were mounted on slides using a mounting medium and stored at 4 °C. Fluorescence images were captured using a confocal scanning laser microscope (SP8, Leica, Germany). Quantitative analysis was conducted using LASX software (Leica, Germany) and was further analyzed with ImageJ software (NIH, USA). For each group, images were obtained from at least five mice. Related spinal regions were manually outlined as regions of interest (ROIs), and the total fluorescent intensities in the ROIs per unit area were calculated. The relative fluorescent intensity was expressed as fold change compared to the control group.

Statistical analysis

Data shown in the graphs represent the means ± S.E.M. Analyses were performed using GraphPad Prism 8 software (GraphPad Software, San Diego, CA, United States). The data distribution was determined using the Shapiro-Wilk normality test and parametric or non-parametric tests were chosen accordingly. Unpaired t-test, One-way or two-way analysis of variance (ANOVA) followed by post hoc test was used as indicated in figure legends. A significance level of $P < 0.05$ was considered statistically significant.

Results

HDAC6 inhibitor ACY-1215 ameliorated neuropathic pain in SNI-operated mice

We initially assessed the effects of the HDAC6 inhibitor on pain thresholds in SNI-operated mice. The HDAC6 inhibitor ACY-1215 (20 mg/kg/day) was administered intraperitoneally for 14 consecutive days to male and female mice (Fig. 1A). The dose administered to the mice corresponds to approximately 100–130 mg per day in humans, adjusted for body weight (20 g/mouse; 60–80 kg/human), and aligns with the dosages utilized in clinical trials (120–160 mg) [39, 40]. Mechanical pain thresholds were measured at various time points, as illustrated in the experimental schematic in Fig. 1A. Both male and female mice exhibited allodynia and mechanical hyperalgesia. Systemic administration of ACY-1215 ameliorated SNI-induced pain starting from Day 7 post-SNI operation, achieving relatively stable efficacy by Day 13 in both male (Fig. 1B) and female mice (Fig. S1).

ACY-1215 increased STAT3 acetylation and decreased its phosphorylation in the spinal cord of SNI-operated mice

Subsequently, we investigated the effect of the HDAC6 inhibitor ACY-1215 on the homeostasis of STAT3 protein acetylation and phosphorylation in the L4-L6 lumbar spinal cord of male mice (Fig. 2A). Compared to the control group, the SNI-operated male mice exhibited elevated levels of Tyr705-phosphorylated STAT3 (p-STAT3) but not of Lys685-acetylated STAT3 (Ac-STAT3) in the spinal cord (Fig. 2B-C). Treatment with ACY-1215 reduced p-STAT3 expression and increased Ac-STAT3 (Fig. 2B-C), but did not alter total STAT3 (t-STAT3) levels (Fig. 2D). ACY-1215 increased STAT3 acetylation and reduced STAT3 phosphorylation (Fig. 2B-C), while not altering HDAC6 expression (Fig. 2E). Elevation of Ac-α-tubulin, a known target of HDAC6, indicates that ACY-1215 inhibits HDAC6's deacetylation function (Fig. 2F). Consistently, immunofluorescent staining results in the spinal dorsal horn of SNI-operated mice showed an increase in p-STAT3 expression, which was mitigated following ACY-1215 treatment (Fig. 2G-H). Additionally, HDAC6 expression remained unchanged after SNI or ACY-1215 treatment (Fig. 2I-J). These results indicate that HDAC6 inhibition modulates the post-translational modification of spinal STAT3 by suppressing its phosphorylation and elevating its acetylation.

HDAC6 and p-STAT3 were expressed in the spinal dorsal Horn neurons

To elucidate the cellular localization of HDAC6 and p-STAT3 in the spinal cord, we performed double immunostaining for HDAC6 and p-STAT3 using three cell-specific markers: GFAP (for astrocytes), NeuN (for neurons), and Iba1 (for microglia) in the spinal cord of

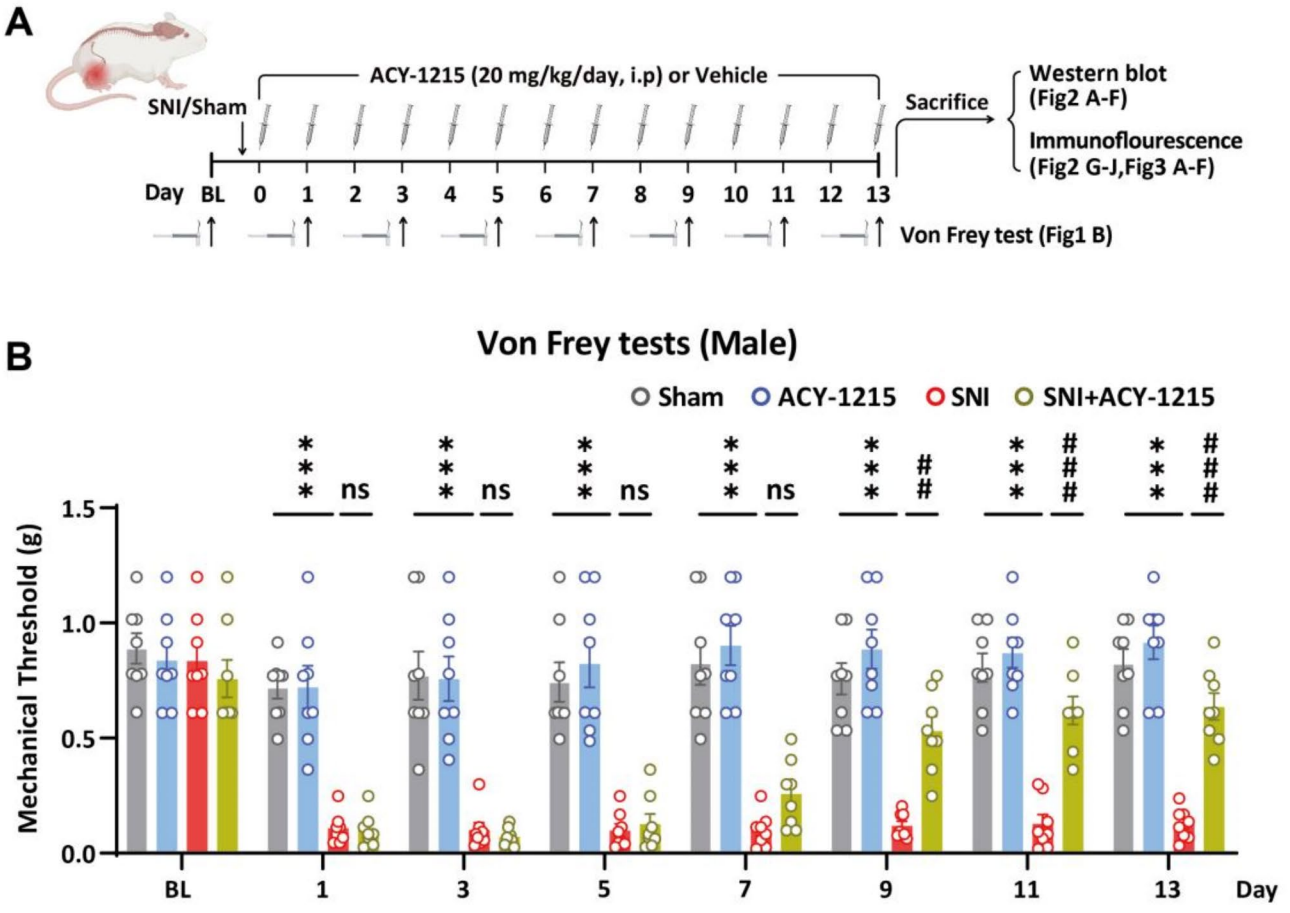

Fig. 1 Histone deacetylase 6 (HDAC6) inhibitor ACY-1215 attenuated mechanical pain in SNI-operated mice. (**A**) The experimental timeline diagram shows the protocol for constructing the SNI mouse model and the administration of treatments. ACY-1215 (20 mg/kg/day) or vehicle (10% DMSO in saline) was administered starting from day 1 post-SNI and continued daily until day 13. Baseline (BL) thresholds were measured one day before any treatment, and mechanical pain thresholds were assessed every two days thereafter. (**B**) Mechanical thresholds for different groups of male mice in von Frey tests. Data are shown as individual values with means ± SEM; $n = 8$ mice per group. RM two-way ANOVA followed by Tukey's post hoc tests. Sham vs. SNI $^{**}p < 0.01$, $^{***}p < 0.001$; SNI vs. SNI + ACY-1215 $^{\#\#}p < 0.01$, $^{\#\#\#}p < 0.001$

SNI-operated mice (Fig. 3A-B). In the spinal dorsal horn, 43% of neurons expressed HDAC6. Additionally, HDAC6 was also detected in astrocytes (SNI: 14%) and microglia (SNI: 12%), albeit to a lesser extent (Fig. 3A-B). Similarly, p-STAT3 also highly co-localized with NeuN (SNI: 54%) and, to a lesser extent, with GFAP (SNI: 19%) and Iba1 (SNI: 14%) (Fig. 3C, D).

Additionally, both HDAC6 (Fig. 3E) and p-STAT3 (Fig. 3F) co-localized with the non-peptidergic nociceptive neuron marker IB4 and the peptidergic nociceptive neuron marker CGRP in lamina I-II of the mouse spinal cord. These findings suggest that HDAC6 and p-STAT3 are expressed in neurons of the dorsal spinal lamina associated with non-peptidergic and peptidergic nociceptive afferent pathway.

Neuropathic pain enhanced nucleus translocation of p-STAT3, not Ac-STAT3

As a transcription factor, active STAT3 exerts its function on gene expression by translocating to the nucleus. Therefore, we evaluated p-STAT3 and Ac-STAT3 levels in the subcellular fractions of spinal cord tissue (Fig. 4A). The SNI operation upregulated nucleus-bound p-STAT3 in the SNI group but did not alter cytosolic p-STAT3 levels in the spinal cord (Fig. 4B-C). Although there was a decreasing trend in cytosolic Ac-STAT3 levels in SNI-operated mice, no significant difference was detected (Fig. 4D). Total STAT3, Ac-α-tubulin, and HDAC6 expression levels were not altered in the cytosol or nuclei following the SNI operation (Fig. 4E-G). Notably, low levels of Ac-STAT3 were detected in the nuclei of the spinal cord of both sham and SNI mice (Fig. 4D), suggesting that the acetylation of STAT3 prevents its translocation into the nucleus.

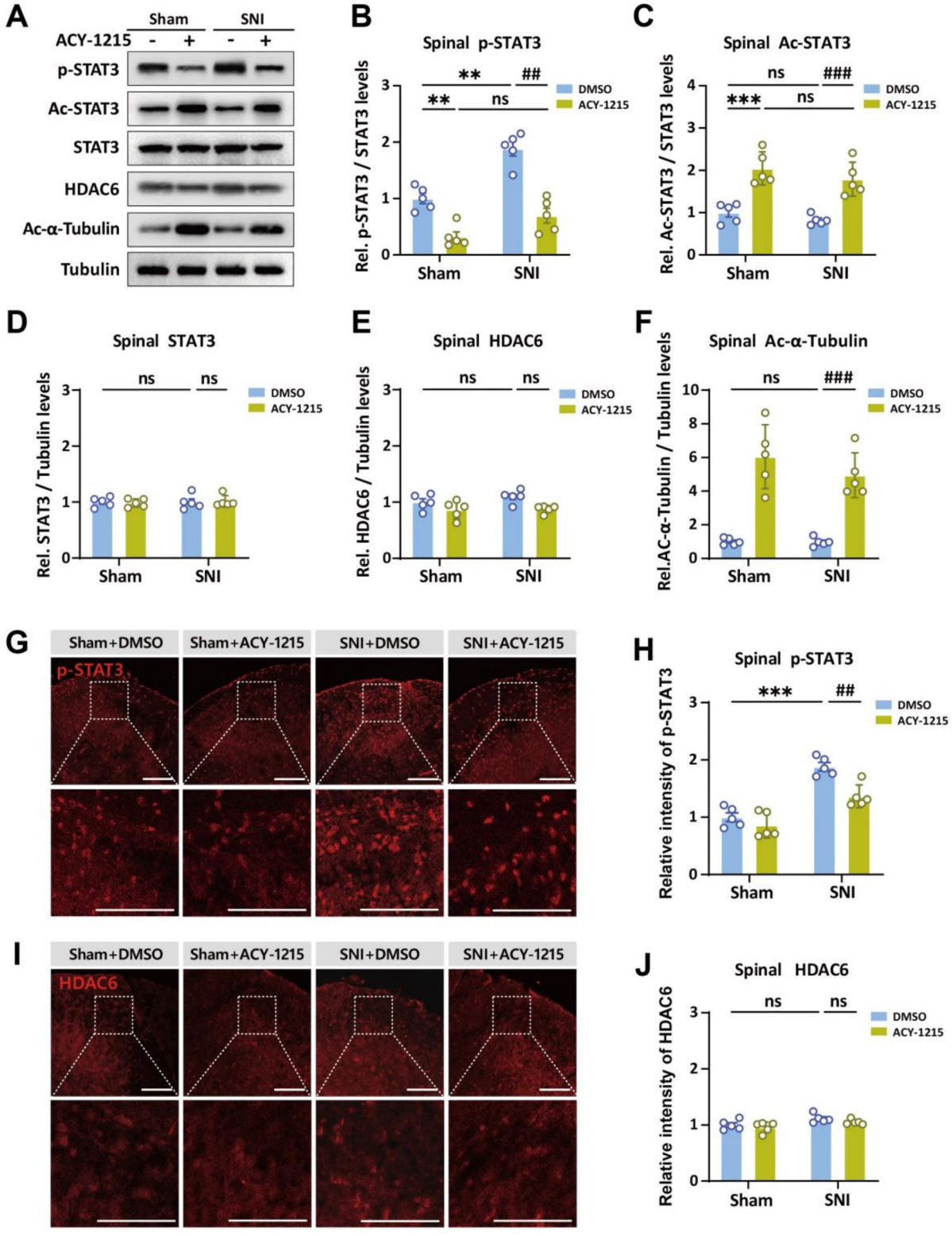

Fig. 2 ACY-1215 increased STAT3 acetylation and decreased its phosphorylation in the spinal cord of SNI-operated mice. (**A**) On the 14th-day post-SNI, L4-L6 spinal cord tissues were collected from mice in the Sham + DMSO, Sham + ACY-1215, SNI + DMSO, and SNI + ACY-1215 groups. Representative blots showing target protein levels in each group. (**B**-**F**) Relative (Rel.) expression levels of p-STAT3 (**B**), Ac-STAT3 (**C**), total STAT3 (**D**), HDAC6 (**E**), and Ac-α-Tubulin (**F**) in each group. Data are presented as means ± SEM. Sham vs. SNI $^{**}p < 0.01$; Sham + DMSO vs. Sham + ACY-1215 $^{**}p < 0.01$, $^{***}p < 0.001$; SNI + DMSO vs. SNI + ACY-1215 $^{\#\#}p < 0.01$, $^{\#\#\#}p < 0.001$; $n = 5$. (**G**-**J**) Immunofluorescent staining of p-STAT3 (**G**-**H**) and HDAC6 (**I**-**J**) in the spinal dorsal horn. Scale bar = 100 μm. The relative intensity is expressed as fold change compared to the sham group treated with DMSO. Data are presented as means ± SEM. Sham + DMSO vs. SNI + DMSO $^{***}p < 0.001$; SNI + DMSO vs. SNI + ACY-1215 $^{\#\#}p < 0.01$; $n = 5$. Two-way ANOVA followed by Tukey's post hoc tests

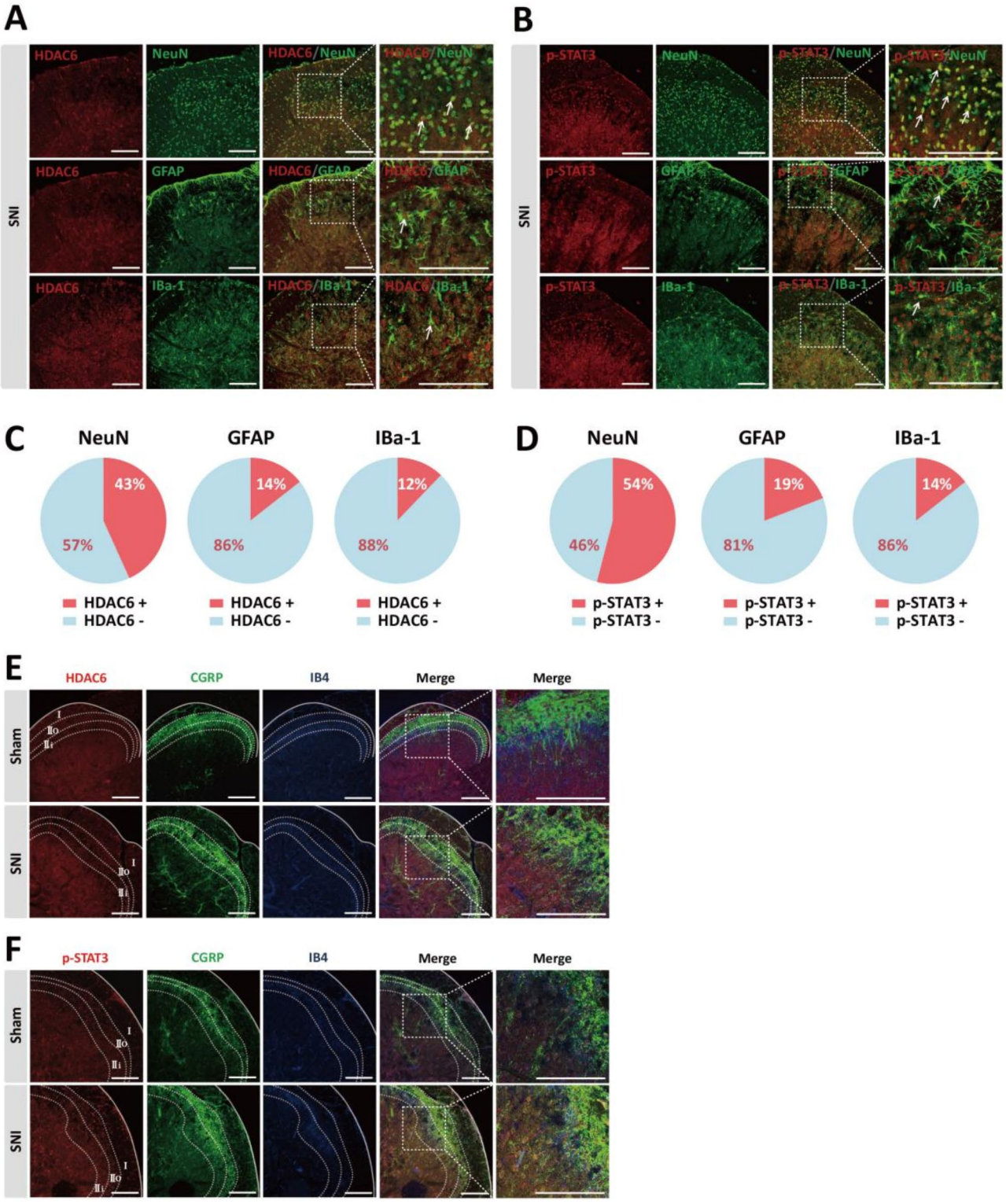

Fig. 3 HDAC6 and p-STAT3 primarily co-localize with NeuN and, to a lesser extent, with GFAP and Iba1 in the L4-L6 dorsal horn of SNI mice. (**A**-**B**) Representative confocal images showing the co-localization of HDAC6 (red, **A**) or p-STAT3 (red, **B**) with NeuN, GFAP, and Iba1 (green) in the spinal dorsal horn of SNI-operated mice. (**C**-**D**) Percentages of HDAC6-positive/negative cells (**C**) and STAT3-positive/negative cells (**D**) in NeuN-, GFAP- and Iba1-positive cells in spinal dorsal horn. (**E**-**F**) Representative images showing the co-localization of HDAC6 (red, **E**) or p-STAT3 (red, **F**) with CGRP (green), and IB4 (blue) in L4-L6 spinal dorsal horn of Sham and SNI-operated mice. Scale bar = 100 μm, $n = 5$

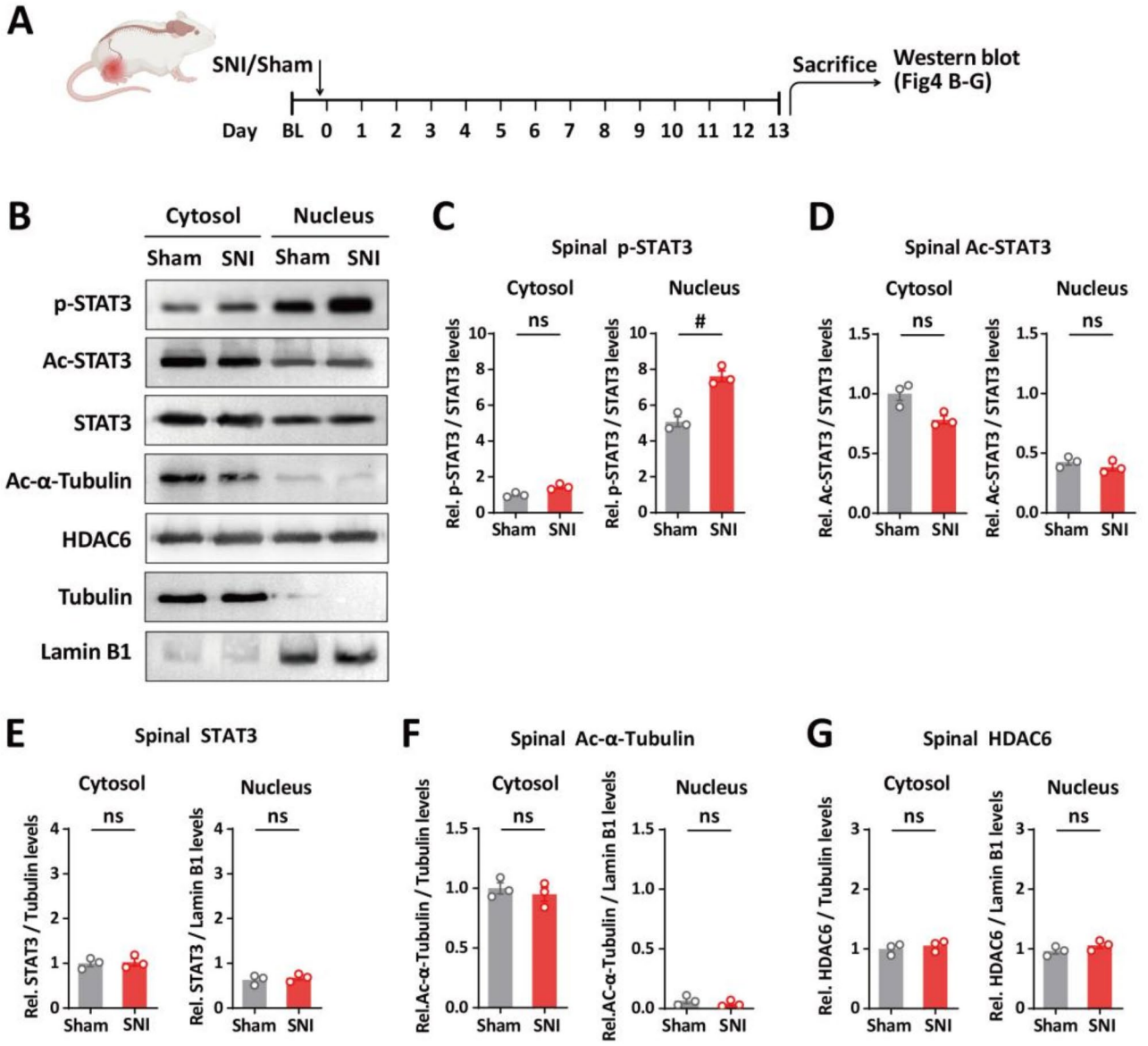

Fig. 4 Neuropathic pain-enhanced nuclear translocation of p-STAT3. (**A**) Subcellular fractionation was performed on spinal cord tissues from sham and SNI groups to obtain cytoplasmic (Cyto) and nuclear (Nuc) fractions. (**B**) Western blot analysis was used to detect protein expression of p-STAT3, Ac-STAT3 and total STAT3 in each fraction. α-Tubulin: cytosolic marker; Lamin B1: nuclear marker. (**C**-**G**) The relative expression levels of spinal p-STAT3 (**C**), Ac-STAT3 (**D**), total STAT3 (**E**), Ac-α-Tubulin (**F**), and HDAC6 (**G**) were quantified relative to STAT3 or tubulin and normalized as fold change compared to sham group. Data are presented as means ± SEM; $n = 3$. Sham vs. SNI, $^{\#}p < 0.05$; Unpaired t-tests

Neuropathic pain enhanced HDAC6-STAT3 interaction, which was decreased by ACY-1215

To investigate whether HDAC6 directly binds STAT3 in the spinal cord, we evaluated the interaction between HDAC6 and STAT3 using co-IP (Fig. 5A). The results indicated that the SNI operation increased the interaction between HDAC6 and STAT3, while ACY-1215 administration reversed the SNI-enhanced spinal HDAC6-STAT3 interaction (Fig. 5B-C). ACY-1215 also increased the acetylation of STAT3 without altering total STAT3 expression levels (Fig. 5D-E).

Neuronal STAT3 overexpression evoked pain hypersensitivity and elevated synthesis of TNF-α and IL-1β,which was reversed by ACY-1215 administration

Previous studies have highlighted the essential role of glial STAT3 in chronic pain, while evidence addressing the role of neuronal STAT3 in the spinal cord is limited. Following the observation of SNI-induced elevation of p-STAT3 expression in spinal neurons, the subsequent examination focused on whether neuronal overexpression of STAT3, driven by a neuron-specific promoter, was sufficient to induce pain. Furthermore, the investigation

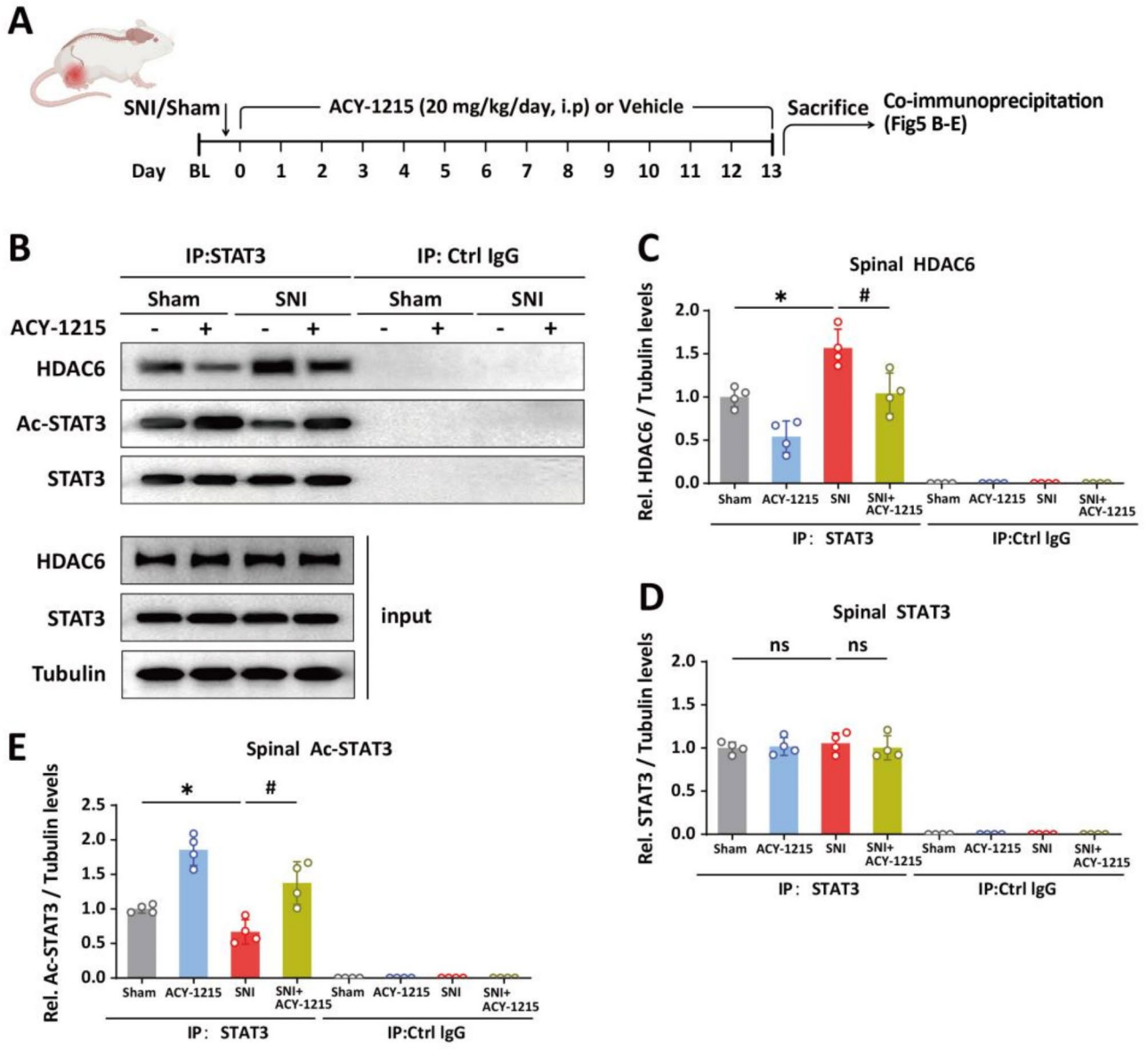

Fig. 5 Neuropathic pain enhanced HDAC6-STAT3 interaction, which was decreased by ACY-1215. (**A**) L4-L6 spinal cord tissues were collected from sham or SNI mice treated with or without ACY-1215. Tissue lysates (input) were immunoprecipitated with anti-STAT3 and immunoblotted for HDAC6, Ac-STAT3, and STAT3. (**B**) Representative western blots of target proteins. (**C**-**E**) Protein levels of HDAC6 (**C**), STAT3 (**D**), and Ac-STAT3 (**E**) in the spinal cord. The values were quantified relative to tubulin and normalized as fold change compared to the sham group receiving vehicle. Data are presented as means ± SEM; $n = 4$, Sham vs. SNI $^{*}p < 0.05$, SNI vs. SNI + ACY-1215 $^{\#}p < 0.05$; one-way ANOVA followed by Tukey's post hoc tests

was extended to ascertain whether ACY-1215 influenced this process (Fig. 6A). The results of behavioral tests showed that intrathecal administration of AAV-hsyn-STAT3 induced mechanical pain hypersensitivity from Day 21 post-administration (Fig. 6B). Systematic administration of ACY-1215 alleviated pain induced by neuronal overexpression of STAT3 (Fig. 6B). The immunoblot assay results indicated that intrathecal administration of AAV-hsyn-STAT3 led to an increase in total STAT3 levels (Fig. 6C-D). This increase subsequently resulted in elevated levels of p-STAT3 and Ac-STAT3 relative to tubulin levels (Fig. 6E-F). The administration of ACY-1215 resulted in suppression of p-STAT3 (Fig. 6E, H) and elevation of Ac-STAT3 (Fig. 6F, I), along with a reduction in the p-STAT3/Ac-STAT3 ratio (Fig. 6G).

A substantial body of evidence underscores the role of STAT3 in elevating the synthesis of pro-inflammatory cytokines, such as TNF-α and IL-1β. Here, we examined the production of TNF-α and IL-1β using immunoblotting (Fig. 6J-L) and ELISA (Fig. 6M-N). The results indicated that ACY-1215 administration reversed the spinal levels of pro-inflammatory cytokines TNF-α (Fig. 6K, M)

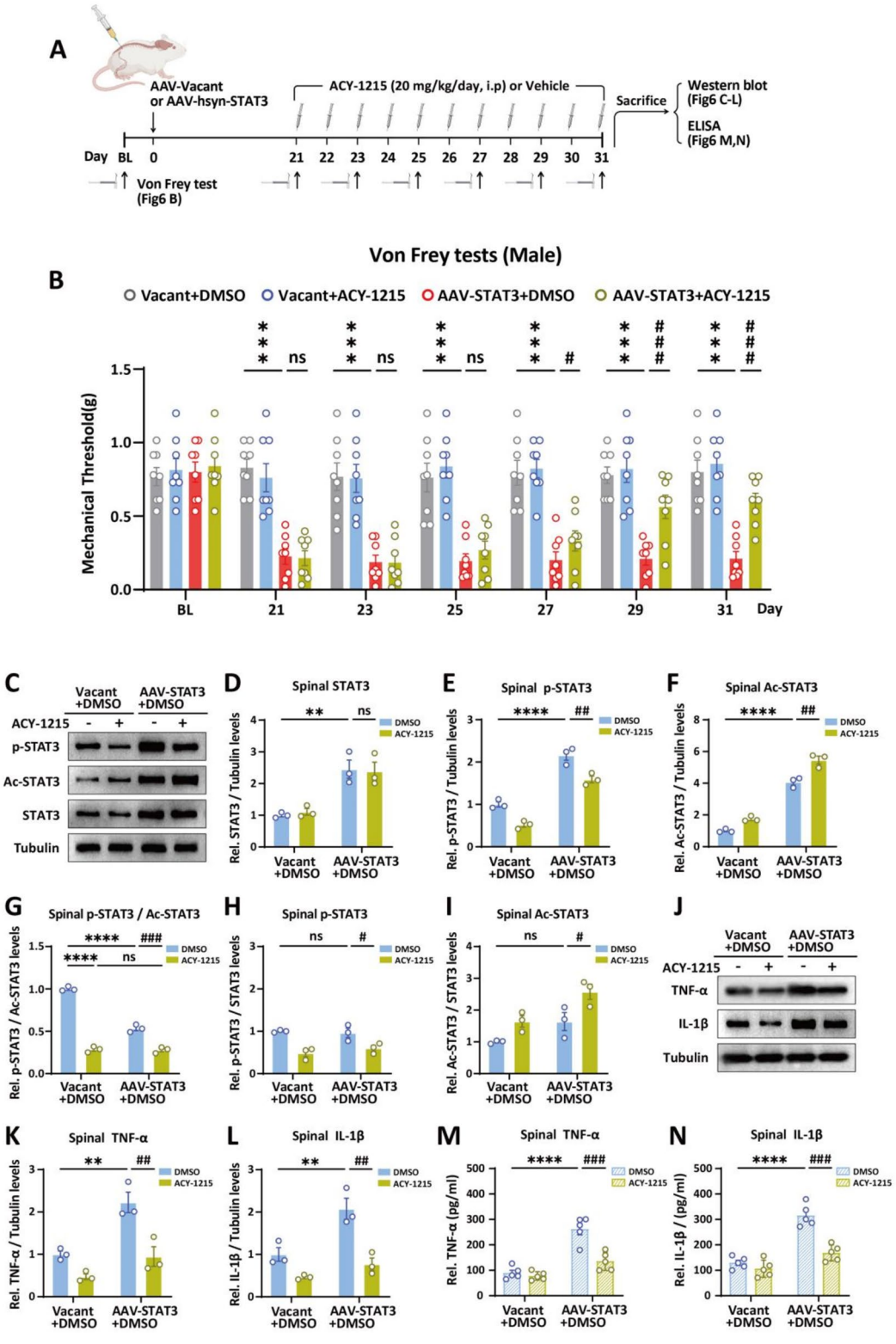

Fig. 6 (See legend on next page.)

(See figure on previous page.)

Fig. 6 Neuronal STAT3 overexpression evoked pain hypersensitivity and elevated synthesis of proinflammatory cytokines, which was reversed by ACY-1215 administration. (**A**) The diagram illustrates the experimental timeline for behavioral and molecular tests following the overexpression of STAT3 in neurons of male mice. Mice were intrathecally injected with AAV-hsyn-STAT3-EGFP (AAV-STAT3) or control AAV virus (Vacant), followed by daily intraperitoneal injections of ACY-1215 or vehicle (10% DMSO in saline) from Day 21 to Day 31. Baseline (BL) thresholds were measured the day preceding any treatment. (**B**) Mechanical threshold and withdrawal latency data for male mice. Two-way ANOVA followed by Tukey's post hoc tests ($n = 8$ mice per group). Data are individual values with means ± SEM. Vacant + DMSO vs. AAV-STAT3 + DMSO $^{***}p < 0.001$; AAV-STAT3 + DMSO vs. AAV-STAT3 + ACY-1215 $^{\#}p < 0.05$, $^{\#\#\#}p < 0.001$. (**C**) Representative western blots of total STAT3, p-STAT3, Ac-STAT3 and tubulin. (D-I) Statistical results showing the relative expressional levels of total STAT3, p-STAT3, Ac-STAT3 and p-STAT3/Ac-STAT3 ratio. (**J**-**L**) Western blots (**J**) and statistical results for protein levels of TNF-α (**K**) and IL-1β (**L**). The blot densities were quantified relative to STAT3 or tubulin and normalized as fold change compared to the AAV-Vacant group receiving DMSO. Values represent mean ± SEM; $n = 3$. Vacant + DMSO vs. AAV-STAT3 + DMSO $^{**}p < 0.01$, $^{****}p < 0.0001$; AAV-STAT3 + DMSO vs. AAV-STAT3 + ACY-1215 $^{\#}p < 0.05$, $^{\#\#}p < 0.01$, $^{\#\#\#}p < 0.001$; Vacant + DMSO vs. Vacant + ACY-1215 $^{****}p < 0.0001$. (**M**-**N**) ELISA analysis of TNF-α (**M**) and IL-1β (**N**) expression levels in L4-L6 spinal cords. Values represent mean ± SEM; $n = 5$. Vacant + DMSO vs. AAV-STAT3 + DMSO $^{****}p < 0.0001$; AAV-STAT3 + DMSO vs. AAV-STAT3 + ACY-1215 $^{\#\#\#}p < 0.001$. Two-way ANOVA followed by Tukey's post hoc tests

and IL-1β (Fig. 6L, N) elevated by neuronal STAT3 overexpression. These findings indicate a regulatory effect of HDAC6 activity on the expression of TNF-α and IL-1β driven by STAT3 overexpression.

ACY-1215 reversed SNI-elevated production of chemokine CCL7 and CXCL13

Studies have shown that STAT3 activation can stimulate the transcription and expression of numerous cytokines and chemokines. To further investigate the key cytokine(s) and chemokine(s) involved in the HDAC6/STAT3 signaling axis, we compared the levels of 27 cytokines and chemokines in spinal cord tissues among the sham, SNI, and SNI + ACY-1215 groups (Fig. 7A-B). The levels of IL-1β, IL-6, TNF-α, CCL7, and BCA-1 were upregulated following the SNI operation and were suppressed by ACY-1215 (Fig. 7C-G). Among these factors, CCL7 exhibited the most pronounced increase following SNI. More importantly, the surge in CCL7 levels was completely ablated by ACY-1215, suggesting a correlation between CCL7 and HDAC6 in the context of neuropathic pain.

HDAC6 knockdown decreased CCL7 and p-STAT3, and increased Ac-STAT3 in mouse neuronal cells

To confirm the effect of HDAC6 on STAT3 activation and CCL7 production in neurons, we knocked down HDAC6 using HDAC6 siRNA in HT22 cells, a mouse hippocampal neuronal cell line (Fig. 8A). We designed an HDAC6 siRNA that effectively suppressed HDAC6 expression in HT22 cells (Fig. 8B-C). The application of HDAC6 siRNA also significantly decreased CCL7 production in both the absence and presence of IL-6, a known STAT3 activator, in HT22 cells (Fig. 8D). Interestingly, we found that IL-6 not only increased p-STAT3 (Fig. 8E-G) but also decreased Ac-STAT3 (Fig. 8H). Treatment with HDAC6 siRNA decreased p-STAT3 (Fig. 8F-G) and increased Ac-STAT3 (Fig. 8H) in both the absence and presence of IL-6 (Fig. 8F-G). The application of HDAC6 siRNA significantly altered the p-STAT3/Ac-STAT3 balance (Fig. 8I) but did not change the total amount of STAT3 (Fig. 8J). These findings suggest a facilitatory effect of HDAC6 on STAT3 activation and CCL7 production.

STAT3 knockdown decreased CCL7 production without affecting HDAC6 in mouse neuronal cells

We also investigated the effect of STAT3 on HDAC6 expression. The designed STAT3 siRNA effectively suppressed total STAT3, p-STAT3, and Ac-STAT3 expression levels relative to tubulin in HT22 cells (Fig. 8K-P). We did not observe an inhibitory effect of STAT3 siRNA on p-STAT3 or Ac-STAT3 relative to total STAT3 due to the low level of total STAT3 (Fig. 8M-O). Importantly, STAT3 siRNA did not affect HDAC6 expression (Fig. 8R) but decreased CCL7 production (Fig. 8S). These findings suggest that HDAC6 is an upstream stimulatory factor of STAT3 activation, and that activation of the HDAC6/STAT3 axis is critical in CCL7 synthesis.

ACY-1215 administration suppressed spinal CCL7, TNF-α and IL-1β production post-SNI operation

We examined the effect of ACY-1215 on production of CCL7, TNF-α, and IL-1β in the spinal cord of sham and SNI-operated mice using immunoblotting (Fig. 9A-F) and ELISA (Fig. 9G-I). Systemic administration of ACY-1215 reversed SNI-elevated STAT3 phosphorylation, as well as CCL7, TNF-α, and IL-1β production, demonstrating the effect of ACY-1215 on STAT3 activation and downstream CCL7 production.

Discussion

In this study, we investigated the effects and mechanisms of HDAC6 inhibition on neuropathic pain using a SNI mouse model. Our findings demonstrate that the selective HDAC6 inhibitor ACY-1215 significantly alleviated SNI-induced mechanical allodynia and hyperalgesia (Fig. 10). ACY-1215 increased acetylation STAT3 acetylation while reducing its phosphorylation in the lumbar spinal cord, suggesting that HDAC6 regulates STAT3 post-translational modifications. The expression of HDAC6 and p-STAT3 in spinal dorsal horn nociceptive neurons support the involvement of the HDAC6/STAT3 axis in pain modulation. Additionally, neuronal

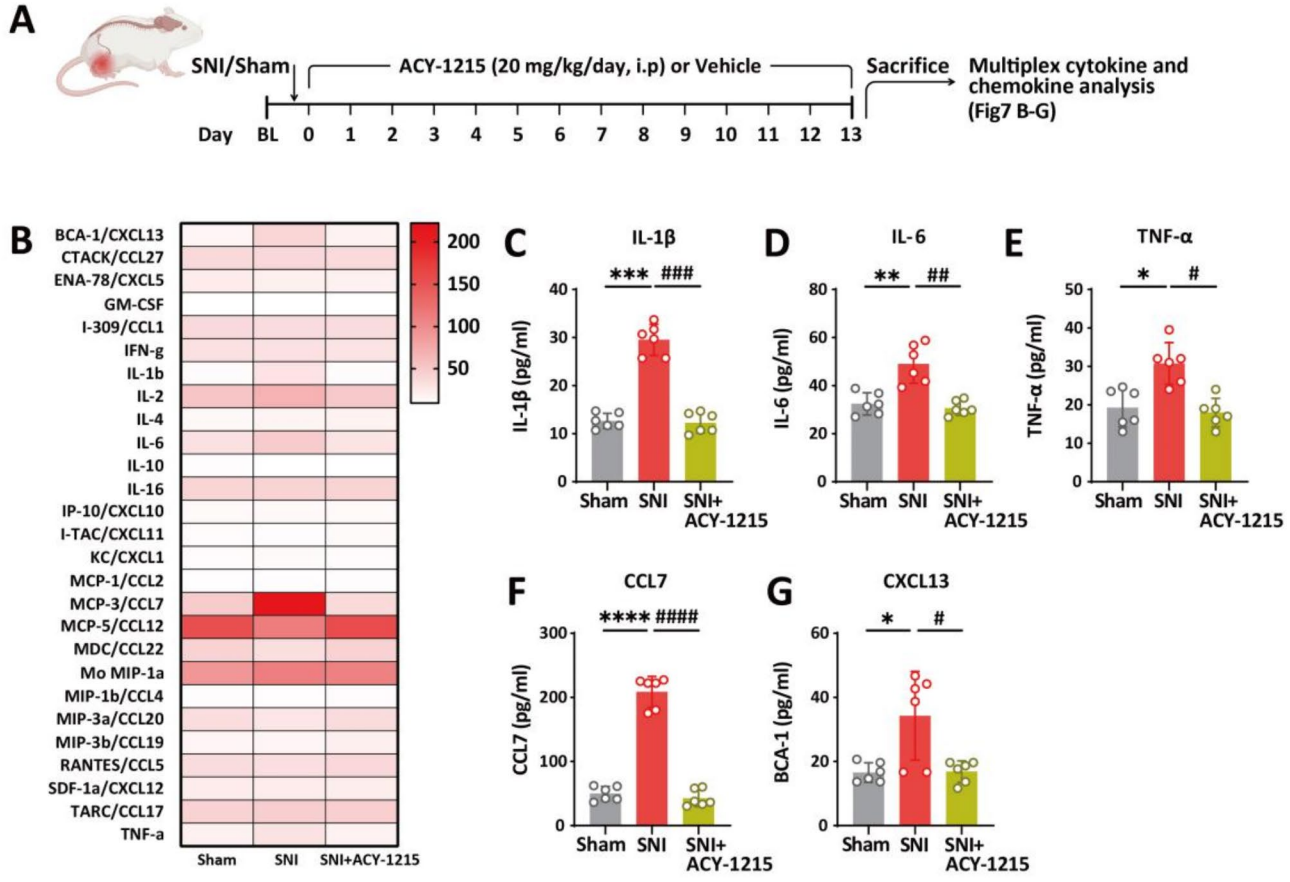

Fig. 7 ACY-1215 reversed SNI-elevated production of chemokine CCL7 and CXCL13. (**A**) The experimental timeline for multiplex cytokine and chemokine analysis. (**B**) Heat map data from multi-factor sequencing analysis of spinal cord tissues from sham + DMSO (Sham), SNI + DMSO (SNI), and SNI + ACY-1215 group mice. Expression levels of IL-1β (**C**), IL-6 (**D**), TNF-α (**E**), CCL7 (**F**), and CXCL13 (**G**) were upregulated in the SNI group compared to the sham group and downregulated in the SNI + ACY-1215 group compared to the SNI group. Data are presented as means ± SEM; $n = 6$. Sham vs. SNI $^{*}p < 0.05$, $^{**}p < 0.01$, $^{***}p < 0.001$, $^{****}p < 0.0001$; SNI vs. SNI + ACY-1215 $^{\#}p < 0.05$, $^{\#\#}p < 0.01$, $^{\#\#\#}p < 0.001$, $^{\#\#\#\#}p < 0.0001$

overexpression of STAT3 induced in pain hypersensitivity and elevated levels of pro-inflammatory cytokines, including CCL7, TNF-α, and IL-1β. The ability of ACY-1215 to suppress these elevations suggests the importance of the HDAC6/STAT3/CCL7 signaling cascade in neuropathic pain and highlights HDAC6 as a potential therapeutic target for neuropathic pain.

Role of HDAC6 Inhibition in STAT3 post-translational modification in neuropathic pain

HDAC6, is distinct from other HDACs by its dual deacetylase domains and specificity for non-histone substrates. While HDAC6 is known to regulate gene transcription via histone deacetylation, it also modulates signaling pathways through acetylation of non-histone proteins such as tubulin, STAT3, and p53 [8, 25].

The activity of STAT3 is predominantly regulated by post-translational modifications and protein-protein interactions [10, 42]. Canonical STAT3 activation involves phosphorylation at Y705 by JAKs, enabling nuclear translocation and transcriptional activation. On the other hand, STAT3 exhibits noncanonical post-translational modifications, such as acetylation and deacetylation. Previous studies have identified K685 as the most well-defined acetylation site in STAT3. Acetylation at Lys685 is facilitated by histone acetyltransferase P300/CBP, while its deacetylation is mediated by HDACs 1, 2, 3, 5, and 6 [10]. However, the role of STAT3 Lys685 acetylation remains controversial. Some reports indicate that acetylation enhances its stability and transcriptional activity [43, 44], while others demonstrate a negative impact of Lys685 acetylation on transcriptional activity in vitro [45]. Notably, Belo et al. found that acetylation alone does not affect the crystal structure, DNA binding affinity, or specificity of STAT3, implying that acetylation-dependent transcriptional activity of STAT3 involves additional factors [46]. Here, we demonstrate that p-STAT3, rather than Ac-STAT3, is the predominant isoform of STAT3 translocated into the nucleus in the spinal cord. Our results indicate that, at least in the spinal

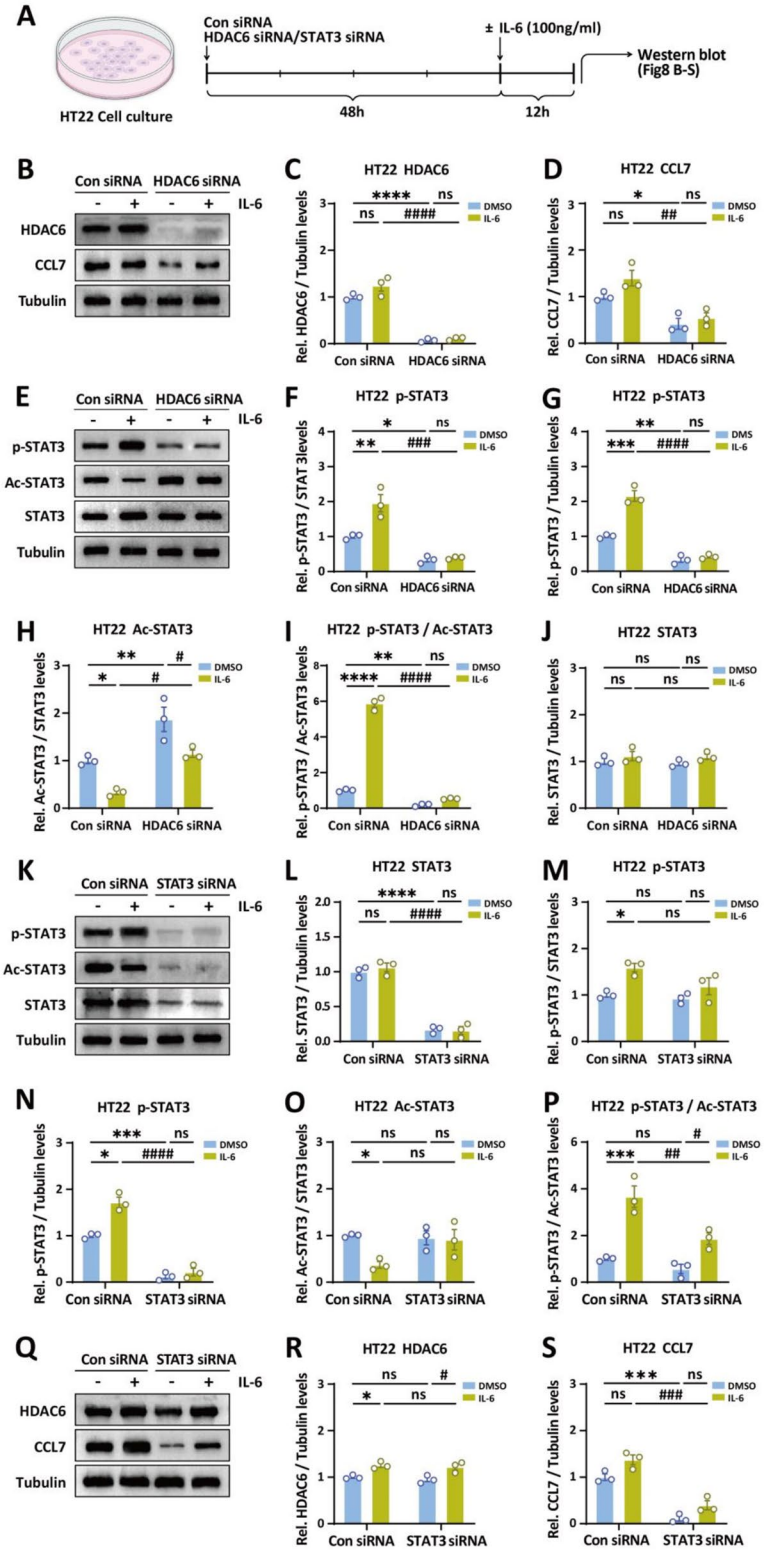

Fig. 8 (See legend on next page.)

(See figure on previous page.)

Fig. 8 HDAC6 knockdown decreased STAT3 phosphorylation and CCL7 production, and STAT3 knockdown decreased CCL7 production without affecting HDAC6 in mouse HT22 neuronal cells in vitro. (**A**) HT22 cells were treated with siRNA specific for HDAC6 or control siRNA for 48 h, followed by incubation with or without 100 ng/ml IL-6 for 12 h. (**B**) Representative western blots of HDAC6, CCL7 and tubulin were displayed. (**C**-**D**) Statistical results of relative expressional levels of HDAC6 (**C**) and CCL7 (**D**), normalized to tubulin. (**E**) Representative western blots of p-STAT3, Ac-STAT3, total STAT3, and tubulin following HDAC6 or control siRNA treatment. (**F**-**J**) Statistical results of relative expressional levels of p-STAT3, Ac-STAT3, p-STAT3/Ac-STAT3, and total STAT3 after HDAC6 or control siRNA treatment. (**K**) Representative western blots of p-STAT3, Ac-STAT3, total STAT3, and tubulin following STAT3 or control siRNA treatment. (**L**-**P**) Statistical results of relative expressional levels of total STAT3, p-STAT3, Ac-STAT3, p-STAT3/Ac-STAT3 after STAT3 or control siRNA treatment. (**Q**-**S**) Representative western blots (**Q**) and statistical results of HDAC6 (**R**), and CCL7 (**S**) protein levels after STAT3 or control siRNA treatment. The blot densities were quantified relative to STAT3 or tubulin and normalized as fold change compared to control HT22 cells treated with control siRNA and DMSO. Data are presented as means ± SEM; $n = 3$. Control siRNA vs. HDAC6 siRNA or STAT3 siRNA $^{*}p < 0.05$, $^{**}p < 0.01$, $^{***}p < 0.001$, $^{****}p < 0.0001$; HDAC6 (or STAT3) siRNA vs. HDAC6 (or STAT3) siRNA + IL-6 $^{\#}p < 0.05$; Control siRNA vs. Control siRNA $^{*}p < 0.05$, $^{**}p < 0.01$, $^{***}p < 0.001$, $^{****}p < 0.0001$; Control siRNA + IL-6 vs. HDAC6 (or STAT3) siRNA + IL-6 $^{\#}p < 0.05$, $^{\#\#}p < 0.01$, $^{\#\#\#}p < 0.001$, $^{\#\#\#\#}p < 0.0001$. Two-way ANOVA followed by Tukey's post hoc tests

cord, STAT3's transcriptional activity is predominantly mediated by p-STAT3, rather than Ac-STAT3.

Our results indicate that the HDAC6 inhibitor ACY-1215 alleviates SNI-induced neuropathic pain by increasing STAT3 acetylation and decreasing its phosphorylation in the lumbar spinal cord without affecting total STAT3 expression. Treatment with either ACY-1215 or HDAC6 siRNA modulates the balance of acetylation and phosphorylation, subsequently inhibiting the nuclear translocation and transcriptional activity of STAT3. This suggests that disrupting HDAC6 activity hinders the maladaptive activation of STAT3 in the context of neuropathic pain, thereby indicating a novel mechanism for HDAC6 inhibitors' anti-nociceptive effects.

Neuronal STAT3 in neuropathic pain

STAT3 is a transcription factor that responds to various extracellular signals and plays a crucial role in regulating gene expression [19, 20]. STAT3 activation has been implicated in glial-mediated neuroinflammation and pain sensitization [21, 24, 47, 48]. However, our study reveals a neuron-specific role for STAT3 in neuropathic pain. HDAC6 and p-STAT3 co-localized with IB4 (non-peptidergic) and CGRP (peptidergic) nociceptive markers in spinal laminae I-II, indicating their expression in dorsal spinal neurons linked to both nociceptive pathways. Previous studies have highlighted that aberrant activation of glial STAT3 elevates production of pro-inflammatory cytokines like TNF-α and IL-1β, which further sensitize nociceptive neurons [49–51]. Our results show that neuronal overexpression of STAT3 induces pain hypersensitivity and elevates TNF-α and IL-1β levels, which are mitigated by ACY-1215. This neuron-specific mechanism underscores the role of neuronal STAT3 in pain transmission and suggest that HDAC6 inhibition may attenuate pain by targeting neuronal rather than glial STAT3 pathways.

CCL7 as a downstream effector of the HDAC6/STAT3 signaling

Our study identifies CCL7 as an important downstream effector of the HDAC6/STAT3 axis in neuropathic pain. CCL7 levels were elevated in the SNI model and suppressed by ACY-1215. In vitro experiments using HT22 neuronal cells confirmed that HDAC6 or STAT3 knockdown reduces CCL7 expression, suggesting a direct regulatory link. A prior study has shown that CCL7 activates JAK2/STAT3 signaling in mouse microglia, leading to inflammatory pain [52]. Our findings extend this by demonstrating that neuronal HDAC6/STAT3 signaling drives CCL7 production, which in turn exacerbates neuroinflammation and pain. ACY-1215 reversed SNI-induced HDAC6/STAT3 interactions, reducing both STAT3 activation and CCL7 synthesis.

Prior studies suggest that CCL7 contributes to chronic pain development [53–55]. Consistently, our data showed that spinal p-STAT3 level was upregulated, along with the downstream inflammatory factors TNF-α, IL-1β, and CCL7 after nerve injury. ACY-1215 treatment downregulated the expression of p-STAT3, TNF-α, IL-1β, and CCL7, indicating that these factors are involved in the anti-nociceptive effects of ACY-1215. These observations align with evidence implicating the contribution of STAT3 activation to neuroinflammation and pain pathogenesis [26, 56].

Clinical implications and future directions

Evidence suggests that ACY-1215 exhibits high biosafety in lymphoma patients and exhibits favorable brain permeability [18], which could benefit the treatment of central nervous system-related disorders. Preclinical studies have support HDAC6 inhibitors' efficacy in neuropathic and inflammatory pain models [13–15]. Our study provides addition evidence exhibiting the role of HDAC6/STAT3 axis in neuropathic pain. Considering the therapeutic potential of HDAC inhibitors in cancer therapy, HDAC inhibitors, including ACY-1215, may offer advantages in cancer-related pain management.

However, this study has limitations. Our investigation was primarily confined to the SNI model, which may not fully replicate the complexities of neuropathic pain in human cases. Future studies should therefore validate these findings in a wider array of pain models, such as cancer pain, chemotherapy-induced peripheral

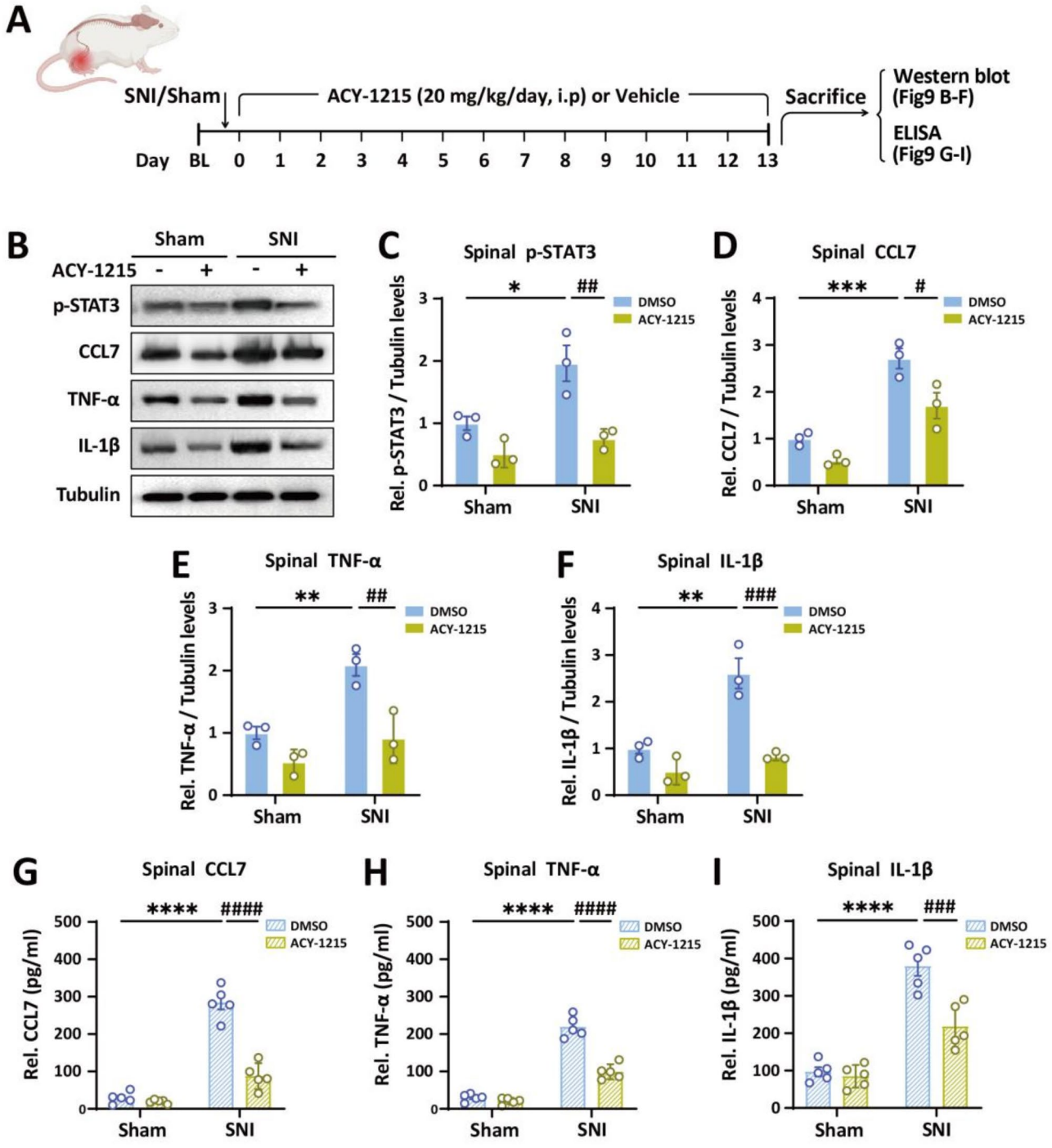

Fig. 9 ACY-1215 administration suppressed spinal CCL7, TNF-α, and IL-1β production post-SNI operation. (**A**) On day 14 post-SNI, L4-L6 spinal cords were collected for western blot analysis and ELISA. (**B**) Representative blots of p-STAT3, TNF-α, IL-1β, and CCL7 in the spinal cord tissue of each group. (**C**-**F**) Protein levels of p-STAT3 (**C**), CCL7 (**D**), TNF-α (**E**), and IL-1β (**F**) were quantified relative to tubulin and further normalized as the fold change compared to the sham group treated DMSO. Values represent mean ± SEM; $n = 3$. Sham vs. SNI $^{*}p < 0.05$, $^{**}p < 0.01$; SNI vs. SNI + ACY-1215 $^{\#}p < 0.05$, $^{\#\#}p < 0.01$, $^{\#\#\#}p < 0.001$. (**G**-**I**) ELISA analysis of CCL7 (**G**) TNF-α (**H**), IL-1β (**I**), and expression levels in L4-L6 spinal cords. Values represent mean ± SEM; $n = 5$. Sham vs. SNI $^{****}p < 0.0001$; SNI vs. SNI + ACY-1215 $^{\#\#\#}p < 0.001$, $^{\#\#\#\#}p < 0.0001$. Two-way ANOVA followed by Tukey's post hoc tests

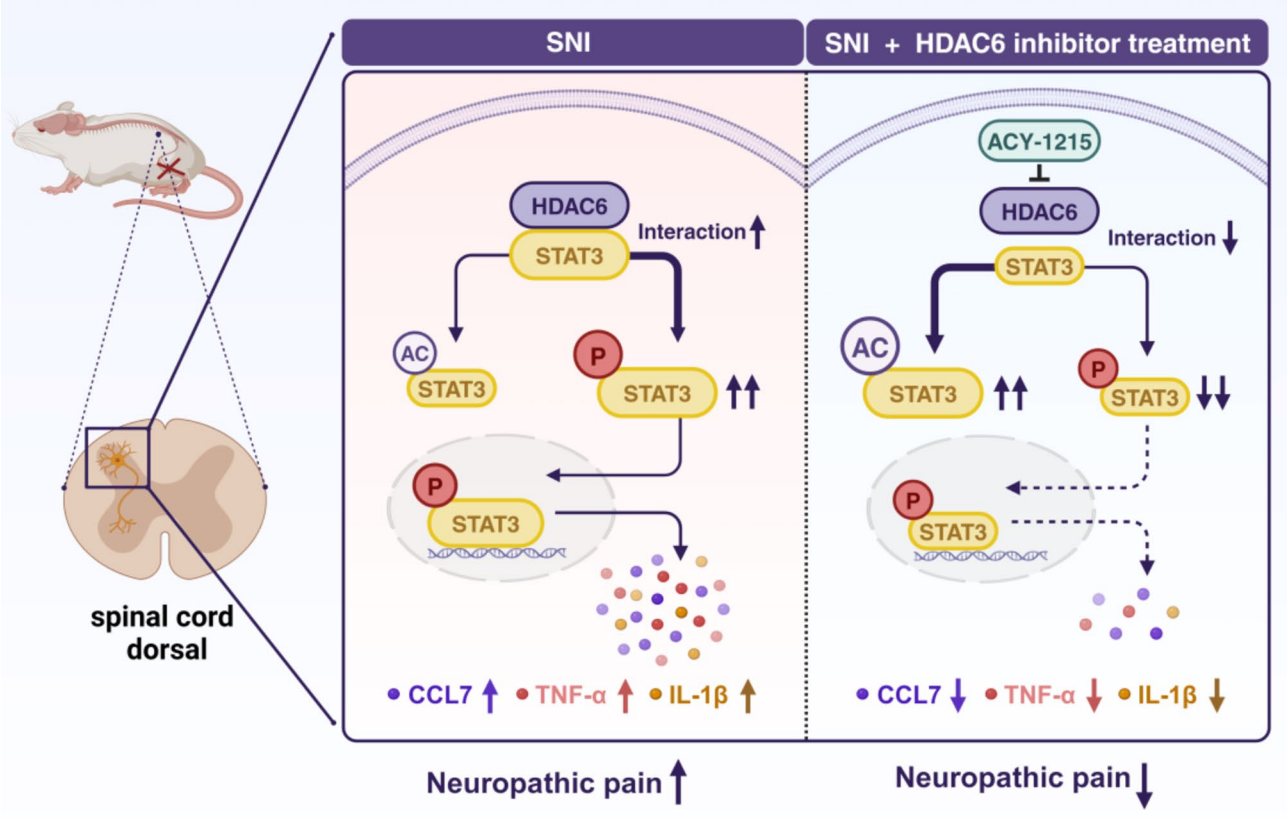

Fig. 10 Schematic summary of HDAC6/STAT3 signaling in neuropathic pain. Left: SNI increases the interaction between HDAC6 and STAT3. HDAC6 regulates STAT3 phosphorylation/acetylation balance and promotes phosphorylation. This enhances STAT3 activity, facilitating its nuclear translocation and subsequent transcription of pro-inflammatory mediators (CCL7, TNF-α, IL-1β) which contribute to neuropathic pain. Right: Treatment with the HDAC6 inhibitor ACY-1215 suppresses HDAC6-STAT3 interaction, increases STAT3 acetylation, and reduces STAT3 phosphorylation. This reduces STAT3 nuclear translocation and the production of CCL7, TNF-α, and IL-1β, thereby alleviating pain

neuropathy, and painful diabetic peripheral neuropathy. Moreover, although we focused on the HDAC6-STAT3 interaction, it is imperative to explore other pathways involved HDAC6's anti-nociceptive actions. Understanding the network of HDAC6 signaling in pain could enhance the therapeutic potential of its inhibitors. Finally, the long-term effects and potential side effects of chronic HDAC6 inhibition on the nervous system have yet to be investigated. Addressing these limitations will be essential to further elucidate the mechanisms and assess the clinical relevance of targeting the HDAC6 pathway.

Conclusion

In conclusion, our study demonstrates that the HDAC6 inhibitor ACY-1215 mitigates neuropathic pain by modulating STAT3 post-translational modifications, reducing its pro-inflammatory signaling, and subsequently suppressing CCL7 production. These findings highlight the therapeutic potential of targeting the HDAC6/STAT3/CCL axis in pain transmission. Further research is needed to translate these preclinical insights into clinical applications.

Supplementary Information

The online version contains supplementary material available at https://doi.org/10.1186/s12974-025-03400-y.

Supplementary Material 1

Supplementary Material 2

Acknowledgements

We thank the technical support of the Core Facilities, Health Science Center, Ningbo University, and Ningbo University Laboratory Animal Center. The cartoon in Fig. 10 was created with BioRender.com.

Author contributions

Zhexi Chi: Formal analysis, Investigation, Visualization, Writing – original draft. Bo Lu: Formal analysis, Investigation, Visualization, Writing – original draft. Chen Pan: Investigation, Formal analysis. Bo Meng: Investigation. Xiuzhong Xing: Investigation. Hui Yuan: Investigation. Xuewei Wu: Investigation. Yushan Chen: Investigation. Yuxuan Ren: Investigation. Wenwei Wu: Investigation. Mengmeng Miao: Investigation. Junping Chen: Supervision, Funding acquisition Writing – review & editing. Xiaowei Chen: Conceptualization, Funding acquisition, Supervision, Investigation, Writing – review & editing.

Funding

This work was supported by National Natural Science Foundation of China (82071239), Zhejiang Provincial Natural Science Foundation of China (LY22H090003), Major program of Ningbo Natural Science Foundation (2022J070). Natural Science Foundation of Ningbo Municipality (Grant No.

2021J309), Ningbo leading medical & health discipline (Grant No. 2022-B10), Ningbo Medical and Health Brand Discipline (PPXK2024-05), Ningbo University's "Double First-Class" Cooperation Special Directional Commissioned Science and Technology Cooperation Project (2403).

Data availability
No datasets were generated or analysed during the current study.

Declarations

Ethics approval
No human subjects were involved in this study. All animal experiments were conducted according to a protocol approved by the Institutional Animal Care and Use Committee of Ningbo University (No.13282).

Competing interests
The authors declare no competing interests.

Received: 30 September 2024 / Accepted: 25 February 2025
Published online: 11 March 2025

References

1. Finnerup NB, Kuner R, Jensen TS. Neuropathic pain: from mechanisms to treatment. Physiol Rev. 2021;101:259–301.
2. van Hecke O, Austin SK, Khan RA, Smith BH, Torrance N. Neuropathic pain in the general population: a systematic review of epidemiological studies. Pain. 2014;155:654–62.
3. Baskozos G, Hébert HL, Pascal MM, Themistocleous AC, Macfarlane GJ, Wynick D, Bennett DL, Smith BH. Epidemiology of neuropathic pain: an analysis of prevalence and associated factors in UK biobank. Pain Rep. 2023;8:e1066.
4. Jensen TS, Finnerup NB. Allodynia and hyperalgesia in neuropathic pain: clinical manifestations and mechanisms. Lancet Neurol. 2014;13:924–35.
5. Attal N. D Bouhassira 2015 Pharmacotherapy of neuropathic pain: which drugs, which treatment algorithms? Pain 156 Suppl 1 S104–14.
6. Jones MR, Urits I, Wolf J, Corrigan D, Colburn L, Peterson E, Williamson A, Viswanath O. Drug-Induced peripheral neuropathy: A narrative review. Curr Clin Pharmacol. 2020;15:38–48.
7. Hubbert C, Guardiola A, Shao R, Kawaguchi Y, Ito A, Nixon A, Yoshida M, Wang XF, Yao TP. HDAC6 is a microtubule-associated deacetylase. Nature. 2002;417:455–8.
8. Chueh AC, Tse JW, Tögel L, Mariadason JM. Mechanisms of histone deacetylase Inhibitor-Regulated gene expression in Cancer cells. Antioxid Redox Signal. 2015;23:66–84.
9. Diallo M, Herrera F. The role of understudied post-translational modifications for the behavior and function of signal transducer and activator of transcription 3. FEBS J. 2022;289:6235–55.
10. Tesoriere A, Dinarello A, Argenton F. The roles of Post-Translational modifications in STAT3 biological activities and functions. Biomedicines 2021, 9.
11. Kaur S, Rajoria P, Chopra M. Ricolinostat suppresses proliferation, promotes apoptosis, and enhances the antiproliferative activity of topoisomerase inhibitors in cervical cancer cells. Drug Dev Res. 2022;83:1822–30. https://doi.org/10.1002/ddr.21999.
12. Seto E, Yoshida M. Erasers of histone acetylation: the histone deacetylase enzymes. Cold Spring Harb Perspect Biol. 2014;6:a018713.
13. Chen C, Liu A, Lu Q, Luo L, Li J, Ke J, Liu Y, Feng X. HDAC6 inhibitor ACY-1215 improves neuropathic pain and its comorbidities in rats of peripheral nerve injury by regulating neuroinflammation. Chem Biol Interact. 2022;353:109803.
14. English K, Barton MC. HDAC6: A key link between mitochondria and development of peripheral neuropathy. Front Mol Neurosci. 2021;14:684714.
15. Sakloth F, Manouras L, Avrampou K, Mitsi V, Serafini RA, Pryce KD, Cogliani V, Berton O, Jarpe M, Zachariou V. HDAC6-selective inhibitors decrease nerve-injury and inflammation-associated mechanical hypersensitivity in mice. Psychopharmacology. 2020;237:2139–49.
16. Zhou S, Huang J, Li K, Du S, Yang B, Guo Z. Genistein attenuates LPS-induced inflammatory injury of rat dorsal root ganglion neuron via down-regulating HDAC6. Zhong Nan Da Xue Xue Bao Yi Xue Ban. 2022;47:707–16.
17. Bahram Sangani N, Koetsier J, Mélius J, Kutmon M, Ehrhart F, Evelo CT, Curfs LMG, Reutelingsperger CP, Eijssen LMT. A novel insight into neurological disorders through HDAC6 protein-protein interactions. Sci Rep. 2024;14:14666.
18. Gu X, Zhang H, Jiao M, Han B, Zhang Z, Li J, Zhang Q. Histone deacetylase 6 inhibitors with blood-brain barrier penetration as a potential strategy for CNS-Disorders therapy. Eur J Med Chem. 2022;229:114090.
19. Dai XY, Liu L, Song FH, Gao SJ, Wu JY, Li DY, Zhang LQ, Liu DQ, Zhou YQ, Mei W. Targeting the JAK2/STAT3 signaling pathway for chronic pain. Aging Dis. 2024;15:186–200.
20. Hu Z, Deng N, Liu K, Zhou N, Sun Y, Zeng W. CNTF-STAT3-IL-6 Axis mediates neuroinflammatory cascade across Schwann Cell-Neuron-Microglia. Cell Rep. 2020;31:107657.
21. Lee JY, Park CS, Seo KJ, Kim IY, Han S, Youn I, Yune TY. IL-6/JAK2/STAT3 axis mediates neuropathic pain by regulating astrocyte and microglia activation after spinal cord injury. Exp Neurol. 2023;370:114576.
22. Liu Y, Feng L, Ren S, Zhang Y, Xue J. Inhibition of LncRNA DILC attenuates neuropathic pain via the SOCS3/JAK2/STAT3 pathway. Biosci Rep 2020, 40.
23. Qin L, Wu X, Block ML, Liu Y, Breese GR, Hong JS, Knapp DJ, Crews FT. Systemic LPS causes chronic neuroinflammation and progressive neurodegeneration. Glia. 2007;55:453–62.
24. Yang B, Zang LE, Cui JW, Zhang MY, Ma X, Wei LL. Melatonin plays a protective role by regulating miR-26a-5p-NRSF and JAK2-STAT3 pathway to improve autophagy, inflammation and oxidative stress of cerebral Ischemia-Reperfusion injury. Drug Des Devel Ther. 2020;14:3177–88.
25. Barter MJ, Butcher A, Wang H, Tsompani D, Galler M, Rumsby EL, Culley KL, Clark IM, Young DA. HDAC6 regulates NF-κB signalling to control chondrocyte IL-1-induced MMP and inflammatory gene expression. Sci Rep. 2022;12:6640.
26. Xu M, Ni H, Xu L, Shen H, Deng H, Wang Y, Yao M. B14 ameliorates bone cancer pain through downregulating spinal interleukin-1β via suppressing neuron JAK2/STAT3 pathway. Mol Pain. 2019;15:1744806919886498.
27. Wang H, Huang C, Zhao L, Zhang H, Yang JM, Luo P, Zhan BX, Pan Q, Li J, Wang BL. Histone deacetylase inhibitors regulate P-gp expression in colorectal cancer via transcriptional activation and mRNA stabilization. Oncotarget. 2016;7:49848–58.
28. Jiang BC, Liu T, Gao YJ. Chemokines in chronic pain: cellular and molecular mechanisms and therapeutic potential. Pharmacol Ther. 2020;212:107581.
29. Wang J, Yin C, Pan Y, Yang Y, Li W, Ni H, Liu B, Nie H, Xu R, Wei H, et al. CXCL13 contributes to chronic pain of a mouse model of CRPS-I via CXCR5-mediated NF-κB activation and pro-inflammatory cytokine production in spinal cord dorsal Horn. J Neuroinflammation. 2023;20:109.
30. Gao Y, Mei C, Chen P, Chen X. The contribution of neuro-immune crosstalk to pain in the peripheral nervous system and the spinal cord. Int Immunopharmacol. 2022;107:108700.
31. Decosterd I, Woolf CJ. Spared nerve injury: an animal model of persistent peripheral neuropathic pain. Pain. 2000;87:149–58.
32. Liu R, Sun D, Xing X, Chen Q, Lu B, Meng B, Yuan H, Mo L, Sheng L, Zheng J, et al. Intranasal Oxytocin alleviates comorbid depressive symptoms in neuropathic pain via elevating hippocampal BDNF production in both female and male mice. Neuropharmacology. 2024;242:109769.
33. Zhu H, Yu Y, Zheng L, Wang L, Li C, Yu J, Wei J, Wang C, Zhang J, Xu S, et al. Chronic inflammatory pain upregulates expression of P2Y2 receptor in small-diameter sensory neurons. Metab Brain Dis. 2015;30:1349–58.
34. Pan C, Xu Y, Jiang Z, Fan C, Chi Z, Zhang Y, Miao M, Ren Y, Wu Z, Xu L, et al. Naringenin relieves Paclitaxel-induced pain by suppressing calcitonin gene-related peptide signalling and enhances the anti-tumour action of Paclitaxel. Br J Pharmacol. 2024;181:3136–59.
35. Mei C, Pan C, Xu L, Miao M, Lu Q, Yu Y, Lin P, Wu W, Ni F, Gao Y, et al. Trimethoxyflavanone relieves Paclitaxel-induced neuropathic pain via inhibiting expression and activation of P2X7 and production of CGRP in mice. Neuropharmacology. 2023;236:109584.
36. Xu F, Yang J, Lu F, Liu R, Zheng J, Zhang J, Cui W, Wang C, Zhou W, Wang Q, et al. Fast Green FCF Alleviates Pain Hypersensitivity and Down-Regulates the Levels of Spinal P2X4 Expression and Pro-inflammatory Cytokines in a Rodent Inflammatory Pain Model. Front Pharmacol. 2018;9:534.
37. Chi Z, Byeon HE, Seo E, Nguyen QT, Lee W, Jeong Y, Choi J, Pandey D, Berkowitz DE, Kim JH, Lee SY. Histone deacetylase 6 inhibitor Tubastatin A attenuates angiotensin II-induced hypertension by preventing cystathionine γ-lyase protein degradation. Pharmacol Res. 2019;146:104281.
38. Chi Z, Le TPH, Lee SK, Guo E, Kim D, Lee S, Seo SY, Lee SY, Kim JH, Lee SY. Honokiol ameliorates angiotensin II-induced hypertension and endothelial dysfunction by inhibiting HDAC6-mediated cystathionine γ-lyase degradation. J Cell Mol Med. 2020;24:10663–76.
39. Amengual JE, Lue JK, Ma H, Lichtenstein R, Shah B, Cremers S, Jones S, Sawas A. First-in-Class selective HDAC6 inhibitor (ACY-1215) has a highly favorable

safety profile in patients with relapsed and refractory lymphoma. Oncologist. 2021;26:184–e366.
40. Cao J, Lv W, Wang L, Xu J, Yuan P, Huang S, He Z, Hu J. Ricolinostat (ACY-1215) suppresses proliferation and promotes apoptosis in esophageal squamous cell carcinoma via miR-30d/PI3K/AKT/mTOR and ERK pathways. Cell Death Dis. 2018;9:817.
41. Hai Y, Christianson DW. Histone deacetylase 6 structure and molecular basis of catalysis and Inhibition. Nat Chem Biol. 2016;12:741–7.
42. Bharadwaj U, Kasembeli MM, Robinson P, Tweardy DJ. Targeting Janus kinases and signal transducer and activator of transcription 3 to treat inflammation, fibrosis, and cancer: rationale, progress, and caution. Pharmacol Rev. 2020;72:486–526.
43. Yuan ZL, Guan YJ, Chatterjee D, Chin YE. Stat3 dimerization regulated by reversible acetylation of a single lysine residue. Science. 2005;307:269–73.
44. Lee JL, Wang MJ, Chen JY. Acetylation and activation of STAT3 mediated by nuclear translocation of CD44. J Cell Biol. 2009;185:949–57.
45. Dasgupta M, Unal H, Willard B, Yang J, Karnik SS, Stark GR. Critical role for lysine 685 in gene expression mediated by transcription factor unphosphorylated STAT3. J Biol Chem. 2014;289:30763–71.
46. Belo Y, Mielko Z, Nudelman H, Afek A, Ben-David O, Shahar A, Zarivach R, Gordan R, Arbely E. Unexpected implications of STAT3 acetylation revealed by genetic encoding of acetyl-lysine. Biochim Biophys Acta Gen Subj. 2019;1863:1343–50.
47. Yu S, Zhao G, Han F, Liang W, Jiao Y, Li Z, Li L. Muscone relieves inflammatory pain by inhibiting microglial activation-mediated inflammatory response via abrogation of the NOX4/JAK2-STAT3 pathway and NLRP3 inflammasome. Int Immunopharmacol. 2020;82:106355.
48. Costigan M, Scholz J, Woolf CJ. Neuropathic pain: a maladaptive response of the nervous system to damage. Annu Rev Neurosci. 2009;32:1–32.
49. Wei X, Huang C, Chen K, Liu S, Wang M, Yang L, Wang Y. BMP7 attenuates neuroinflammation after spinal cord injury by suppressing the microglia activation and inducing microglial polarization via the STAT3 pathway. Neurochem Res. 2023;48:2687–700.
50. Imai S, Ikegami D, Yamashita A, Shimizu T, Narita M, Niikura K, Furuya M, Kobayashi Y, Miyashita K, Okutsu D, et al. Epigenetic transcriptional activation of monocyte chemotactic protein 3 contributes to long-lasting neuropathic pain. Brain. 2013;136:828–43.
51. Ke BC, Huang XX, Li Y, Li LY, Xu QX, Gao Y, Liu Y, Luo J. Neuronal-derived Ccl7 drives neuropathic pain by promoting astrocyte proliferation. NeuroReport. 2016;27:849–57.
52. Park J, Kim Y, Lee C, Kim YT. 3,5-Dicaffeoylquinic acid attenuates microglial activation-mediated inflammatory pain by enhancing autophagy through the suppression of MCP3/JAK2/STAT3 signaling. Biomed Pharmacother. 2022;153:113549.
53. Kwiatkowski K, Popiolek-Barczyk K, Piotrowska A, Rojewska E, Ciapała K, Makuch W, Mika J. Chemokines CCL2 and CCL7, but not CCL12, play a significant role in the development of pain-related behavior and opioid-induced analgesia. Cytokine. 2019;119:202–13.
54. Li J, Deng G, Wang H, Yang M, Yang R, Li X, Zhang X, Yuan H. Interleukin-1β pre-treated bone marrow stromal cells alleviate neuropathic pain through CCL7-mediated Inhibition of microglial activation in the spinal cord. Sci Rep. 2017;7:42260.
55. Zhu LP, Xu ML, Yuan BT, Ma LJ, Gao YJ. Chemokine CCL7 mediates trigeminal neuropathic pain via CCR2/CCR3-ERK pathway in the trigeminal ganglion of mice. Mol Pain. 2023;19:17448069231169373.
56. Molet J, Mauborgne A, Diallo M, Armand V, Geny D, Villanueva L, Boucher Y, Pohl M. Microglial Janus kinase/signal transduction and activator of transcription 3 pathway activity directly impacts astrocyte and spinal neuron characteristics. J Neurochem. 2016;136:133–47.

Publisher's note